Hindawi
Advances in Civil Engineering
Volume 2021, Article ID 8867741, 8 pages
https://doi.org/10.1155/2021/8867741

Research Article

Laboratory Investigation on Particle Breakage Characteristics of Calcareous Sands

Qingsheng Chen,[1] **Wan Peng**,[1] **Ronghu Yu**,[1] **Gaoliang Tao**,[1,2] **and Sanjay Nimbalkar**[3]

[1]*Hubei Provincial Ecological Road Engineering Technology Research Center, Hubei University of Technology, Wuhan 430068, China*
[2]*School of Urban Construction, Wuchang University of Technology, Wuhan 430223, China*
[3]*School of Civil and Environmental Engineering, University of Technology Sydney, 15 Broadway, Ultimo NSW 2007, Australia*

Correspondence should be addressed to Qingsheng Chen; chqsh2006@163.com and Gaoliang Tao; tgl1979@126.com

Received 24 March 2020; Revised 19 February 2021; Accepted 28 February 2021; Published 9 March 2021

Academic Editor: Xiaodong Hu

Many studies have demonstrated the fragility of calcareous sands even under small stresses. This bears an adverse influence on their engineering properties. A series of laboratory tests were carried out on poor-graded calcareous sands to investigate the crushability mechanism. Einav's relative breakage and fractal dimension were used as the particle breakage indices. The results show that the particles broke into smaller fragments at the low-stress level by attrition which was caused by friction and slip between particles. In contrast, particles broke in the form of crushing at the relatively higher stresses. The evolution of the particle size was reflected by the variation in Einav's relative breakage and fractal dimension. As testing commenced, the breakage index rapidly increased. When the stress was increased to 400 kPa, the rate of increase in the breakage index was retarded. As the stress was further increased beyond 800 kPa, the rate of increase in the fractal index became much smaller. This elucidated that the well-graded calcareous sands could resist crushing depending on the range of applied stresses. Based on the test findings, a new breakage law is proposed.

1. Introduction

Calcareous sands are rich in calcium carbonate or other insoluble carbonate products. These sands are mainly distributed in the continental shelf, the coastline of the tropical/subtropical climate between latitude 30° north and 30° south, the Southern China Sea, and the Red Sea. Calcareous sands differ from those sourced from land in terms of the particle shapes, internal porous structure, and the mechanical properties [1, 2]. Owing to such variations, the particles are easy to crumble even under the small stresses [3–6]. In the field, the engineering structures constructed on the calcareous sand are prone to undergo large differential settlement. Therefore, it is of paramount importance to study the breakage mechanism of the calcareous sand particles.

Particle breakage can significantly affect the strength [7–11], permeability, and deformation [12–15] of coarse-grained soils and can increase the uncertainty on the efficacy of engineering applications. Many studies dealing with particle breakage assessment have been proposed in the past [16, 17]. Yu [18] explained the effect of particle fragmentation in calcareous sand by its effect on consolidation and shear properties, friction, and shear-induced volumetric expansion of coral sand. Wang et al. [19] found that irregularity in particle shape is a prerequisite for the generation of particle breakage in calcareous soils. Although the relative crushing rate defined by Hardin [20] is widely used [21–26], the concept of relative breakage is yet to be fully explored. Einav [27] assumed that soil particles would undergo complete fragmentation in the shear process and defined the relative breakage in terms of the relative distance of the current grain size distribution from the initial and ultimate distributions. He modified Hardin's crushing index to put forward the relative fragmentation rate suitable for

granular soil particles. Some scholars determined the particle size distribution before and after the particle breakage of soil based on the fractal theory [26–28]. Hence, it is feasible to quantitatively describe the particle breakage based on the relative breaking rate and the fractal dimension.

Internationally, scholars have adopted a wide range of methodologies/tools to study the crushing mechanism of calcified sand particles, including cyclic triaxial shearing [29], under drained and undrained triaxial compression [30], dynamic image analysis [31], and uniaxial compression [32], among others. In this paper, the uniaxial compression tests were carried out on the poor-graded calcareous sands collected from the Southern China Sea. The particles before and after the testing were screened to obtain the change in particle size distributions. The influence of the consolidation stress on the crushing of the calcareous sands particles was analyzed. The micromorphology of calcareous sands with a single particle size was studied by scanning electron microscope (SEM) tests, and the mode of particle breakage was described. By using the fractal dimension and Einav's breakage rate, the grain breakage under the confined compression testing was quantified. The breakage characteristics of the calcareous sand under different vertical stresses were assessed. The present study has the potential to serve as a useful design guide for the structures founded on calcareous sands.

2. Test Materials and Method

The calcareous sand used in this study was collected from the reef in Nansha Island, China. The calcareous sand consisted of coral broken branches and biological debris which had the calcium carbonate content as high as 90%. Figure 1 shows the images of characteristic particles of calcareous sands. Before the test, the calcareous sand was washed and air-dried. The particles larger than 4 mm in size were removed to minimize the effects of boundary conditions on test results. The particle size distribution curve of calcareous sand is shown in Figure 2, which represents poor gradation. The relative density of the sand sample was obtained by the pycnometer test. The physical characteristics are summarized in Table 1.

The compression test was carried out by using consolidation apparatus as shown in Figure 3. The samples were prepared in-ring knife samples of 61.8 mm × 20 mm. The rate of deformation was controlled as 0.01 mm per hour as per the industry standard (GB/T50123, 1999). The calcareous sand was subjected to compression tests at seven different levels of vertical stress (50, 100, 200, 400, 800, 1600, and 3200 kPa). The sample was sieved after the completion of compression that lasted for 36 h. The screening of calcareous sand particles below 0.25 mm in size was ignored.

Scanning electron microscope (SEM) tests were conducted to observe the microscopic images of the original calcareous sand with different particle sizes (4, 3, 2, 1, 0.5, and 0.25 mm). In this experiment, the sputtering speed is 10 mm/min and the sputtering time is 60 s. SEM diagrams of samples are shown in Figures 4 and 5.

3. Test Results

The particle size distribution of the calcareous sand samples before and after tests was obtained. Figure 6 represents the comparison between the particle size distribution under different stress levels.

It was found that the percentage of coarser particles decreased (while increasing the amount of finer fraction) as the stress increased. This indicated the increased amount of breakage in coarser particles as the stress level increased. Under each incremental stress level, the fraction of particles smaller than 1 mm increased mainly attributing to the breakage of bigger particles. For the stress below 400 kPa, the percentage mass of medium-sized particles (size 1–2 mm) appeared to vary, while as the stress exceeded 800 kPa, the amount of medium-size particles increased. The large particles were crushed after being compressed and split into several medium- to smaller-sized particles. The large-sized particles undergo more breakage compared with smaller particles. This is due to their primary role in stress transfer and development of large contact stresses resulting from the relatively smaller number of interparticulate contact areas available for the force-transfer. Under the low-stress levels below 400 kPa, the finer grains occupy the empty void spaces around coarser particles during particle reorientation and rearrangement thereby inducing grain breakage. Besides, the presence of a large number of asperities evident in coarse angular particles makes them prone to breakage due to intensive stress concentrations developed around the asperities. The dependence of particle shape on the particle size has been discussed earlier [33, 34]. According to the data plotted in Figure 6, the coarser particles above 2 mm were crushed even at the low-stress level of 50 kPa. With the increase in stress, the larger amount of finer fraction implied the substantial particle crushing. This is consistent with the results of existing studies [35].

Figures 4 and 5 are the SEM diagrams of calcareous sand particles with single particle size. It was found that the surfaces of calcareous sands were irregular and the internal structure was porous. This was evident from the compression test data in which the increased stresses led to a larger finer fraction. The particle breakage at low-stress level was in the form of attrition or crushing caused by friction and slip between particles (refer to the location indicated in Figure 4), as well as the particle splitting as a result of specimen compression occurred at the high-stress level.

4. Particle Breakage Index

In order to evaluate the degree of particle breakage of calcareous sands after compression, two parameters, viz., particle fractal dimension and Einav's relative breakage rate, were selected. The particle fractal dimension increased with the increased fine fraction. For the calcareous sand subjected to elevated stress, the particles with large size reduced due to evolution of breakage. Thus, the change in the fractal dimension of a particle could indicate the measure of its breakage. The calcareous sands used in this paper are granular material, and the relative breakage rate proposed by

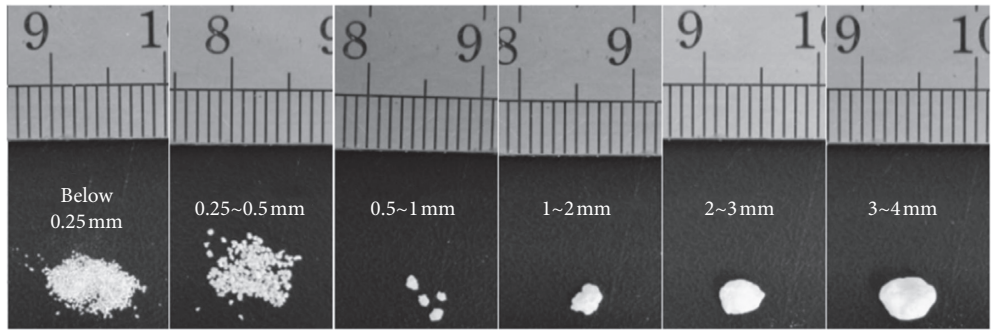

Figure 1: Characteristic particle photographs of calcareous sand.

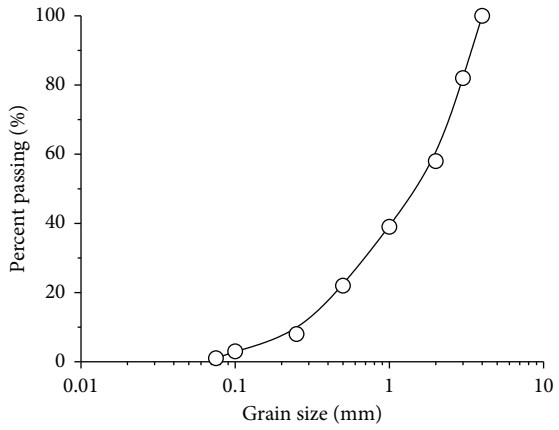

Figure 2: Grain size distribution curve of calcareous sand.

Table 1: Physical parameters of calcareous sand.

Location	Gs	$d10$ (mm)	$d30$ (mm)	$d60$ (mm)	Cu	Cc
Nansha Island	2.77	0.29	0.74	2.92	10.20	0.65

Einav [27] is suitable for describing the breaking degree of calcareous sands.

4.1. Fractal Dimension. A large number of studies have shown that geotechnical media represents obvious fractal features [36–43]. The use of the weight distribution of the particle sizes is therefore appropriate. Based on the Sierpinski carpet (Sierpinski carpet) and the Menger sponge (Menger sponge) fractal model, Tyler and Wheatcraft [44] proposed the relationship between the soil smaller than certain particle size and the fractal dimension of particles:

$$\frac{M(r<R)}{M_T}=\left(\frac{R}{R_{\max}}\right)^{3-D}, \tag{1}$$

where R is the particle size, $R_{\max}$ is the maximum particle size, M is the mass of the particle size range of 0~R, and M_T is the total mass of soil.

By taking the logarithm of both sides of Equation (1), the fractal model could be rewritten as

Figure 3: Consolidation test apparatus.

$$\ln\left[\frac{M(r<R)}{M_T}\right]=(3-D)\ln\left(\frac{R}{R_{\max}}\right). \tag{2}$$

By plotting $\ln(M(r<R)/M_T)$ against $\ln(R/R_{\max})$, $(3-D)$ can be evaluated from the gradient k of the graph and then the fractal dimension can be determined as $D=3-k$. The fitting results are shown in Table 2.

To obtain the relationship between the particle fractal dimension of the sample under different stresses, it is assumed that the particle fractal dimension before crushing is D_b, the particle fractal dimension after crushing is D_a, and the stress is P. The linear regression analysis is then performed on D_a/D_b and P/P_a where P_a is the atmospheric pressure, as shown in Figure 7. It is shown that a significant linear relationship exists between D_a/D_b and P/P_a ($R^2=0.98$). The ratio D_a/D_b can be expressed as follows:

$$\frac{D_a}{D_b}=1.002\left(\frac{P}{P_a}\right)^{0.0004}. \tag{3}$$

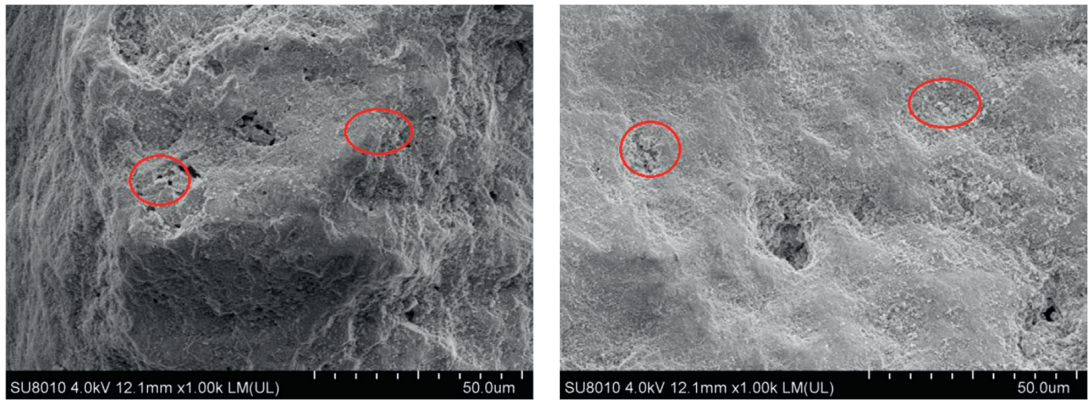

(a) (b)

Figure 4: SEM image in a single grain size calcareous sand particle at an amplification factor of 1000: (a) 0.5–0.25 mm and (b) 0.25–0 mm.

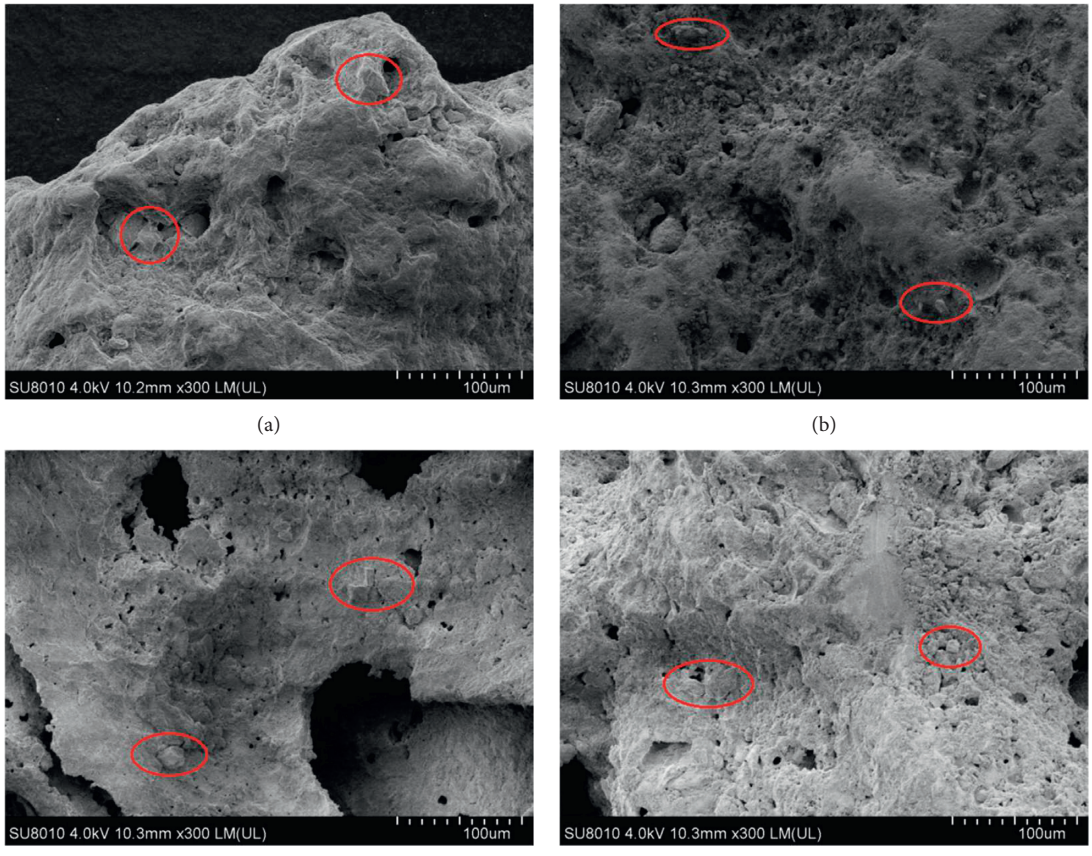

(a) (b)

(c) (d)

Figure 5: SEM images in a single grain size calcareous sand particle at an amplification factor of 300: (a) 1–0.5 mm, (b) 2–1 mm, (c) 3–2 mm, and (d) 4–3 mm.

4.2. Einav's Relative Breakage. The definition of Einav's relative breakage [27] is shown in Figure 8. Based on the relative breakage proposed by Hardin, Einav defined the area of initial distribution $F_0(d)$ to ultimate distribution $F_u(d)$ as B_p. The area of initial distribution $F_0(d)$ to current distribution $F(d)$ is expressed as B_t. Einav's relative breakage can be determined by

$$B_r = \frac{B_t}{B_p} = \frac{\int_{d_m}^{d_M} (F(d) - F_0(d)) d^{-1} d\, d}{\int_{d_m}^{d_M} (F_u(d) - F_0(d)) d^{-1} d\, d} = \frac{S_{\mathrm{ABCA}}}{S_{\mathrm{ABDA}}}, \quad (4)$$

where dM is the maximum particle size and dm is the minimum particle size.

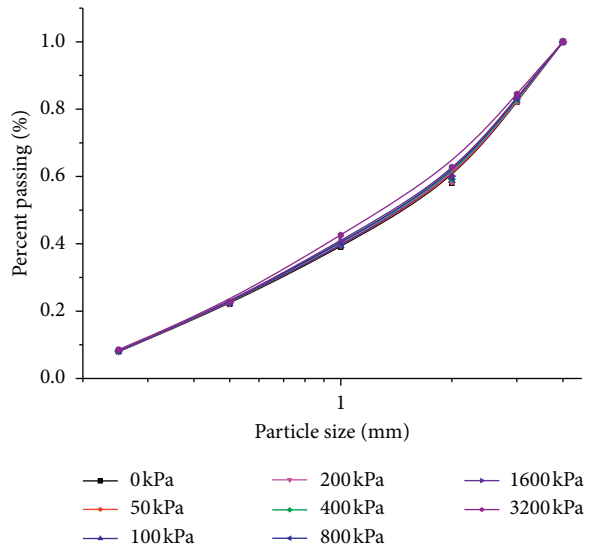

Figure 6: Comparison between the particle size distribution under different stress levels.

Table 2: Fractal dimension D of calcareous sand samples at each stress level.

Stress P (kPa)	Fitting equation	Correlation coefficient R^2	Fractal dimension D
0	$\ln(M(r<R)/M_T) = (3-2.1098)\ln(R/R_{max})$	0.9663	2.1098
50	$\ln(M(r<R)/M_T) = (3-2.1133)\ln(R/R_{max})$	0.9658	2.1133
100	$\ln(M(r<R)/M_T) = (3-2.1139)\ln(R/R_{max})$	0.9662	2.1139
200	$\ln(M(r<R)/M_T) = (3-2.1143)\ln(R/R_{max})$	0.9639	2.1143
400	$\ln(M(r<R)/M_T) = (3-2.1150)\ln(R/R_{max})$	0.9641	2.1150
800	$\ln(M(r<R)/M_T) = (3-2.1153)\ln(R/R_{max})$	0.9652	2.1153
1600	$\ln(M(r<R)/M_T) = (3-2.1165)\ln(R/R_{max})$	0.9647	2.1165
3200	$\ln(M(r<R)/M_T) = (3-2.1170)\ln(R/R_{max})$	0.9657	2.1170

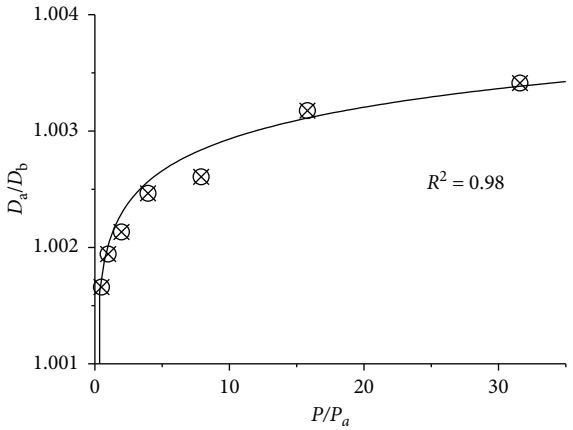

Figure 7: Linear fitting curves for $(D)_a/(D)_b$ and $(P)/(P)_a$.

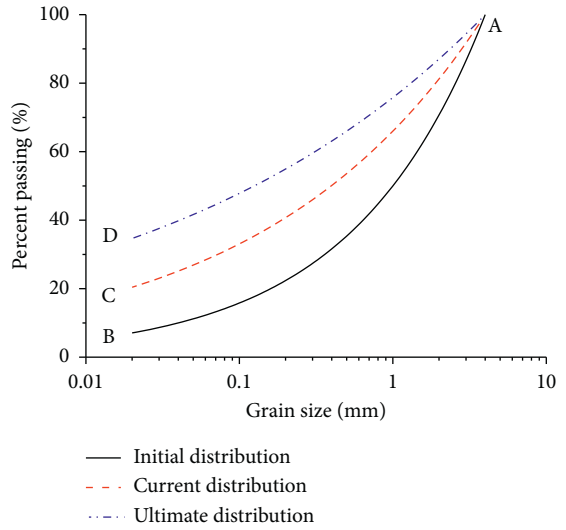

Figure 8: The diagram of Einav's relative breakage.

Combined with Equation (4), Einav's relative breakages under different stress were calculated. Table 3 shows the values of Einav's relative breakage corresponding to each stress level.

Figure 9 shows the relationships between the fractal dimension, Einav's relative breakage, and the vertical stress, respectively. It was seen that the breakage indices, fractal dimension, and Einav's relative breakage showed a rapid increase at an initial stage of compression (the slope of this section is k_1). As the stress continued to increase to 400 kPa, the rate of increase in breakage reduced (the slope of this section is k_2). When the stress exceeded 800 kPa, the increasing rate of breakage declined gradually (the slope of this

Table 3: Einav's relative breakage of calcareous sand samples at each stress level.

Stress (kPa)	50	100	200	400	800	1600	3200
Br (%)	0.03	0.06	0.07	0.1	0.13	0.18	0.34

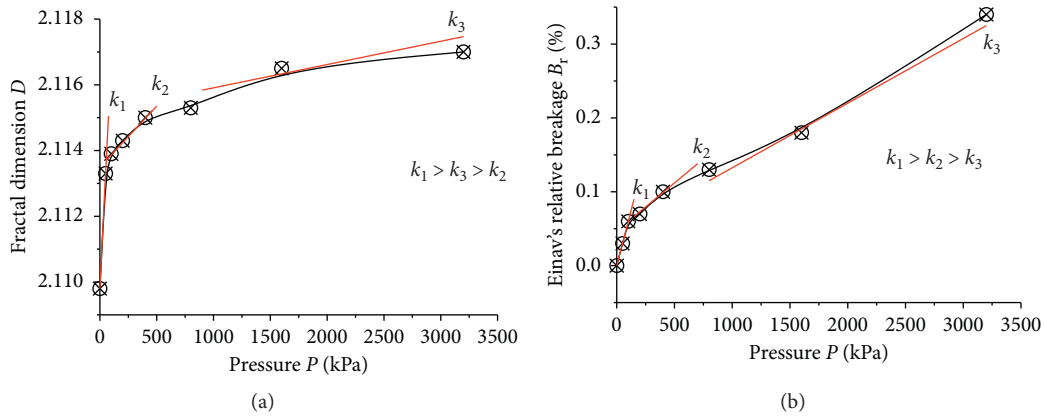

Figure 9: Relationship between breaking indexes and vertical stress (P): (a) fractal dimension (D); (b) Einav's relative breakage.

section is k_3). It was evident that the slope of each following stage became steeper (i.e., $k_1 > k_2 > k_3$), which indicated that the increase in breakage was the most obvious during the initial stage of loading. However, the change in breakage index under subsequent incremental stress level was small. Under the small incremental stress, only a small portion of coarser particles underwent crushing (caused by friction and slip between particles), while the amount of finer particles remained relatively unchanged. It also indicated that within a certain stress range, the well-graded calcareous sand could resist crushing. But if the stress continued to increase, a large number of particles underwent breakage. However, as evident from Figure 9, the stress had a great influence on the initial state of samples (sudden change in value of breakage index), which also showed that calcareous sand at each stress level is accompanied by particle breakage, even at the low-stress level of 50 kPa. This could be verified by the variation in amount of large particles before and after compression testing of calcareous sand as evident from Figure 6.

According to the breakage data listed in Tables 2 and 3, the relationship between Einav's relative breakage and fractal dimension is plotted in Figure 10. It could be seen that all test points fell in a much narrower band, indicating a unique relationship between Einav's relative breakage and the fractal dimension exist although the stress states of different test points are different. This relationship could be expressed using the following power function:

$$D_a = a \times Br^b, \tag{5}$$

where a and b are constant. For the calcareous sand, a is 2.119 and b is 7.901×10^{-4}. It is evident that D and Br have some intrinsic relation; therefore, it is reasonable to take fractal dimension D as a quantitative index of particle breakage [45].

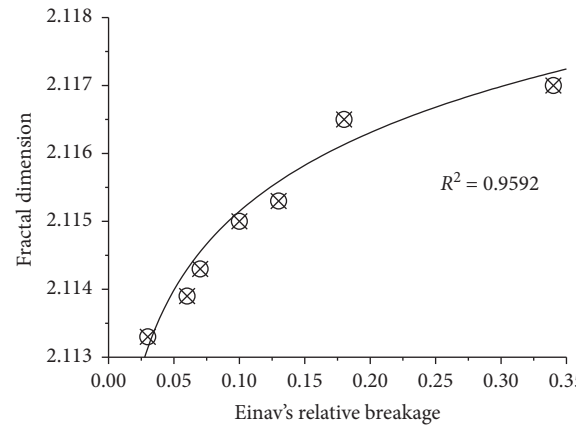

Figure 10: Relationship between Einav's relative breakage and fractal dimension.

The relation between fractal dimension before crushing and Einav's relative breakage can be captured by substituting Equation (3) into (5):

$$D_b\left[1.002\left(\frac{P}{P_a}\right)^{0.0004}\right] = a \times Br^b. \tag{6}$$

Einav's relative breakage of calcareous sand under different stresses can be estimated by Equation (6) when the fractal dimension before crushing and fitting parameters a and b is known. Because the fragility of calcareous sand particles posed challenges in the construction of airport runway and other projects on Southern China Sea islands and reefs, the present study is beneficial to the construction of islands and reefs in the Southern China Sea and the value of local materials.

5. Conclusions

Particle breakage of calcareous sands occurs under small stresses commonly encountered in the field. A series of laboratory tests were performed to determine the breakage law of calcareous sands under such small stresses. The fractal fitting of the laboratory test data and the determination of Einav's relative breakage were carried out. The main findings of the study are summarized as follows:

(1) At the low-stress level, two modes of particle breakage, viz, attrition and crushing (caused by the friction and slippage between the particles) of particles occurred. In contrast, splitting in larger particles occurred at a relatively higher stress level.

(2) The stress had a great influence on the initial state of calcareous sand (increased breakage at initial loading stage), which showed that calcareous sand at each stress level is accompanied by particle breakage, even at the low-stress level of 50 kPa.

(3) The variation in the breakage indices, Einav's relative breakage, and fractal dimension both implied the increase in finer fraction. At the outset of testing, substantial particle breakage was evident which then continued to occur as the stress increased to 400 kPa. The amount of particle breakage was then gradually reduced as the stress increased beyond 800 kPa. The rate of increase became smaller, which showed that the well-graded calcareous sand could resist breakage.

Data Availability

The data used to support the findings of this study are included within the supplementary information files.

Conflicts of Interest

The authors declare that they have no conflicts of interest.

Acknowledgments

The research was funded by the National Natural Science Foundation of China (no. 51708189).

Supplementary Materials

S1 table corresponds to Figure 2. S2 table corresponds to Figure 7(a). S3 table corresponds to Figure 7(b). S4 table corresponds to Figure 8. (*Supplementary Materials*)

References

[1] Z. Q. Yang, W. Zhao, and Z. J. Song, "Geotechnical investigation of calcareous soils," *Rock and Soil Mechanics*, vol. 15, no. 4, pp. 53–60, 1994.

[2] C. Q. Liu and R. Wang, "Preliminary research on physical and mechanical properties of calcareous sand," *Rock and Soil Mechanics*, vol. 19, no. 1, pp. 32–37, 1998.

[3] J. P. Wu, Y. Chu, and Z. G. Lou, "Influence of particle breakage on deformation and strength properties of calcareous sands," *Chinese Journal of Geotechnical Engineering*, vol. 19, no. 5, pp. 49–55, 1997.

[4] J. Z. Sun and R. Wang, "Influence of confined pressure on particle breakage and shear expansion of calcareous sand," *Chinese Journal of Rock Mechanics and Engineering*, vol. 23, no. 4, pp. 641–644, 2002.

[5] J. Z. Sun and R. Wang, "Study on particle failure process of calcareous sand under triaxial compression," *Rock and Soil Mechanics*, vol. 24, no. 5, pp. 822–825, 2003.

[6] J. M. Zhang, L. Zhang, H. Liu, J. J. Wang, and Q. Y. Rui, "Experimental research on shear behaviour of calcareous sand," *Chinese Journal of Rock Mechanics and Engineering*, vol. 27, no. 1, pp. 3010–3015, 2008.

[7] J. F. Wang and H. B. Yan, "On the role of particle breakage in the shear failure behavior of granular soils by DEM," *International Journal for Numerical and Analytical Methods in Geomechanics*, vol. 37, no. 8, pp. 823–854, 2011.

[8] F.-w. Yu and L.-j. Su, "Particle breakage and the mobilized drained shear strengths of sand," *Journal of Mountain Science*, vol. 13, no. 8, pp. 1481–1488, 2016.

[9] Y. Xiao, H. L. Liu, Q. S. Chen, Q. Ma, Y. Xiang, and Y. Zheng, "Particle breakage and deformation of carbonate sands with wide range of densities during compression loading process," *Acta Geotechnica*, vol. 12, no. 5, pp. 1177–1184, 2017.

[10] F. W. Yu, "Characteristics of particle breakage of sand in triaxial shear," *Powder Technology*, vol. 320, Article ID S0032591017306459, 2017.

[11] Y. Xiao, L. Long, T. M. Evans, H. Zhou, H. Liu, and A. W. Stuedlein, "Effect of particle shape on stress-dilatancy responses of medium-dense sands," *Journal of Geotechnical and Geoenvironmental Engineering*, vol. 145, no. 2, Article ID 04018105, 2019.

[12] D. Z. Kong, B. Y. Zhang, and X. Sun, "Triaxial tests on particle breakage strain of artificial rockfill materials," *Chinese Journal of Geotechnical Engineering*, vol. 31, no. 3, pp. 464–469, 2009.

[13] M. Ghafghazi, D. A. Shuttle, and J. T. Dejong, "Particle breakage and the critical state of sand," *Soils and Foundations*, vol. 54, no. 3, pp. 451–461, 2014.

[14] H. D. Chen, H. Z. Wei, Z. Feng, and Y. J. Zhou, "Study on strength and particle shape of calcareous sand particle," *Soil Engineering and Foundation*, vol. 32, no. 6, pp. 637–641, 2018.

[15] Y. Xiao, M. Meng, A. Daouadji, Q. Chen, Z. Wu, and X. Jiang, "Effect of particle size on crushing and deformation behaviors of rockfill materials," *Geoscience Frontiers*, vol. 11, 2019.

[16] Y. Wang, S. Zhang, D. H. Ao, Y. Z. Yu, and X. Sun, "Particle breakage characteristics of rockfills under complex stress paths," *Chinese Journal of Geotechnical Engineering*, vol. 40, no. 4, pp. 698–706, 2018.

[17] R. J. Marsal, "Mechanical properties of rockfill," *Embankment Dam Engineering*, Wiley, New York, NY, USA, 1973.

[18] F. Yu, "Influence of particle breakage on behavior of coral sands in triaxial tests," *International Journal of Geomechanics*, vol. 19, no. 12, p. 04019131, 2019.

[19] X. Wang, Y. Weng, H. Wei, Q. Meng, and M. Hu, "Particle obstruction and crushing of dredged calcareous soil in the Nansha Islands, South China Sea," *Engineering Geology*, vol. 261, p. 105274, 2019.

[20] B. O. Hardin, "Crushing of soil particles," *Journal of Geotechnical Engineering, ASCE*, vol. 111, no. 10, 1985.

[21] K. L. Lee and I. Farhoomand, "Compressibility and crushing of granular soils in anisotropic triaxial compression," *Canadian Geotechnical Journal*, vol. 4, no. 1, pp. 68–86, 1967.

[22] N. Miura and S. O-hara, "Particle-crushing of a decomposed granite soil under shear stresses," *Soils and Foundations*, vol. 19, no. 3, pp. 1–14, 1979.

[23] S. Wei, J. G. Zhu, Q. H. Qian, and F. Li, "Particle breakage of coarse-grained materials in triaxial tests," *Chinese Journal of Geotechnical Engineering*, vol. 31, no. 4, pp. 533–538, 2009.

[24] J. R. Zhang, B. W. Zhang, Y. Hu, and H. X. Liao, "Predicting the particle breakage of granular geomaterials," *Chinese Journal of Rock Mechanics and Engineering*, vol. 35, no. 9, pp. 1898–1905, 2016.

[25] S. Li, F. S. Liu, X. Dai, and Y. L. Zhang, "Study on engineering properties of sand with different calcium carbonate contents," *Chinese Journal of Rock Mechanics and Engineering*, vol. 38, no. 1, pp. 3271–3278, 2019.

[26] Y. Peng, X. M. Ding, Y. Xiao, J. Chu, and W. T. Deng, "Study of particle breakage behaviour of calcareous sand by dyeing tracking and particle image segmentation method," *Rock and Soil Mechanics*, vol. 40, no. 7, pp. 2663–2672, 2019.

[27] I. Einav, "Breakage mechanics-Part I: theory," *Journal of the Mechanics and Physics of Solids*, vol. 55, no. 6, pp. 1274–1297, 2007.

[28] J. Du, K. P. Hou, and G. C. Peng, "Experimental study of compaction characteristics and fractal feature in crushing of coarse-grained soils," *Rock and Soil Mechanics*, vol. 34, no. S1, pp. 155–161, 2013.

[29] G. Wang and J. Zha, "Particle breakage evolution during cyclic triaxial shearing of a carbonate sand," *Soil Dynamics and Earthquake Engineering*, vol. 138, Article ID 106326, 2020.

[30] G. Wang, Z. Wang, Q. Ye, and X. Wei, "Particle breakage and deformation behavior of carbonate sand under drained and undrained triaxial compression," *International Journal of Geomechanics*, vol. 20, no. 3, Article ID 04020012, 2020.

[31] H. Wei, T. Zhao, Q. Meng, X. Wang, and B. Zhang, "Quantifying the morphology of calcareous sands by dynamic image analysis," *International Journal of Geomechanics*, vol. 20, no. 4, Article ID 04020020, 2020.

[32] Y. Wu, H. Yamamoto, J. Cui, and H. Cheng, "Influence of load mode on particle crushing characteristics of silica sand at high stresses," *International Journal of Geomechanics*, vol. 20, no. 3, Article ID 4019194, 2020.

[33] Y. Sun, S. Nimbalkar, and C. Chen, "Particle breakage of granular materials during sample preparation," *Journal of Rock Mechanics and Geotechnical Engineering*, vol. 11, no. 2, pp. 417–422, 2019.

[34] L. M. Le Pen, W. Powrie, A. Zervos, S. Ahmed, and S. Aingaran, "Dependence of shape on particle size for a crushed rock railway ballast," *Granular Matter*, vol. 15, no. 6, pp. 849–861, 2013.

[35] X.-Z. Wang, Y. Weng, H. Wei, Q. Meng, and M. Hu, "Particle obstruction and crushing of dredged calcareous soil in the Nansha Islands, South China Sea," *Engineering Geology*, vol. 261, Article ID 105274, 2020.

[36] G. Tao, Y. Chen, L. Kong, H. Xiao, Q. Chen, and Y. Xia, "A simple fractal-based model for soil-water characteristic curves incorporating effects of initial void ratios," *Energies*, vol. 11, no. 6, p. 1419, 2018.

[37] G. X. Wang, H. W. Huang, and S. F. Xiao, "Experimental study on micro-structural characteristics of soft soil," *Journal of Hydraulic Engineering*, vol. 36, no. 2, pp. 0190–0196, 2005.

[38] G. L. Tao, X. K. Wu, H. L. Xiao, Q. Chen, and J. Cai, "A unified fractal model for permeability coefficient of unsaturated soil," *Fractals*, vol. 27, no. 1, Article ID 1940012, 2019.

[39] Y. Q. Zhou and B. N. Hong, "Experimental research on microstructure changes of clayey soil in process of compression," *Rock and Soil Mechanics*, vol. 26, no. 5, pp. 82–86, 2005.

[40] Y. Yang, H. L. Yao, and S. Y. Chen, "Characteristics of microcosmic structure of Guangxi expansive soil," *Rock and Soil Mechanics*, vol. 27, no. 1, pp. 155–158, 2006.

[41] G. L. Tao, X. L. Zhu, J. C. Cai, H. L. Xiao, Q. Chen, and Y. Chen, "A fractal approach for predicting unsaturated hydraulic conductivity of deformable clay," *Geofluids*, vol. 2019, Article ID 8013851, 9 pages, 2019.

[42] T. Wang, C. Ding, G. Zhao, and T. Ren, "A fast calculation method of thermodynamic properties of variable-composition natural gas mixtures in the supercritical pressure region based on implicit curve-fitting," *Journal of Natural Gas Science and Engineering*, vol. 43, pp. 96–109, 2017.

[43] G. L. Tao, W. Peng, H. L. Xiao, X. K. Wu, and Y. Chen, "Numerical simulation and microscopic stress mechanism for the microscopic pore deformation during soil compression," *Advances in Civil Engineering*, vol. 2019, Article ID 1542797, 14 pages, 2019.

[44] S. W. Tyler and S. W. Wheatcraft, "Fractal scaling of soil particle-size distributions: analysis and limitations," *Soil Science Society of America Journal*, vol. 56, no. 2, pp. 362–369, 1992.

[45] X. S. Shi and Z. L. Cheng, "Fractal behavior in crushing of rockfill material," *Chinese Journal of Rock Mechanics and Engineering*, vol. 29, no. 2, pp. 3852–3857, 2010.